

## Article

# Photoelectronic Properties of Chiral Self-Assembled Diphenylalanine Nanotubes: A Computational Study

Vladimir Bystrov <sup>1,\*</sup>, Ekaterina Paramonova <sup>1</sup>, Pavel Zelenovskii <sup>2,3</sup>, Svitlana Kopyl <sup>2</sup>, Hong Shen <sup>4</sup>, Tie Lin <sup>4</sup> and Vladimir Fridkin <sup>5</sup>

<sup>1</sup> Institute of Mathematical Problems of Biology—Branch of Keldysh Institute of Applied Mathematics, Russian Academy of Sciences, 142290 Pushchino, Russia

<sup>2</sup> Department of Physics & CICECO-Aveiro Institute of Materials, University of Aveiro, 3810-193 Aveiro, Portugal

<sup>3</sup> School of Natural Sciences and Mathematics, Ural Federal University, 620000 Ekaterinburg, Russia

<sup>4</sup> Shanghai Institute of Technical Physics, Chinese Academy of Sciences, Shanghai 200083, China

<sup>5</sup> Shubnikov Institute of Crystallography, Federal Scientific Research Center “Crystallography and Photonics” of Russian Academy of Sciences, 119333 Moscow, Russia

\* Correspondence: vsbys@mail.ru or bystrov@impb.ru

**Abstract:** Peptide nanotubes (PNT) of diphenylalanine (FF) have attracted considerable attention from researchers in the last decades. The chirality of FF monomers determines the kinetics of PNTs’ self-assembly and their morphology. The helical symmetry of PNTs causes significant intrinsic polarization and endows them with a unique combination of mechanical, electronic, and optical properties, as well as a strong piezoelectric effect useful for various applications. In this work, we used a combination of computer modeling and quantum chemical calculations to study the photoelectronic properties of FF PNTs of different chiralities. Using semiempirical methods implemented in the HyperChem and MOPAC packages, we calculated HOMO and LUMO energy levels and a band gap and their variations under the action of external and internal electric fields. We demonstrated that the photoelectronic properties of L- and D-FF PNTs are slightly different and may be related to the intrinsic electric field arising due to the internal polarization. The band gap of FF PNTs is within the ultraviolet range (400–250 nm) and can be tuned by an external electric field. These results open a way to create FF PNT-based solar-blind ultraviolet photodetectors and other electro-optic and electronic devices.

**Keywords:** peptide nanotubes; diphenylalanine; chirality; photoelectronic properties; computer simulation



**Citation:** Bystrov, V.; Paramonova, E.; Zelenovskii, P.; Kopyl, S.; Shen, H.; Lin, T.; Fridkin, V. Photoelectronic Properties of Chiral Self-Assembled Diphenylalanine Nanotubes: A Computational Study. *Symmetry* **2023**, *15*, 504. <https://doi.org/10.3390/sym15020504>

Academic Editors: Anthony Harriman, Victor Borovkov and Sergei D. Odintsov

Received: 28 December 2022

Revised: 28 January 2023

Accepted: 8 February 2023

Published: 14 February 2023



**Copyright:** © 2023 by the authors. Licensee MDPI, Basel, Switzerland. This article is an open access article distributed under the terms and conditions of the Creative Commons Attribution (CC BY) license (<https://creativecommons.org/licenses/by/4.0/>).

## 1. Introduction

For a long time, the identity of the physical and chemical properties of enantiomers was considered an indisputable fact. However, an obvious predominance of biological homochirality has always been in contradiction with this concept [1]. Although the difference between enantiomers is observed mainly in their interaction with other chiral objects, such as other molecules, circularly polarized light, or chiral magnetic and electric fields [1–3], their intrinsic properties (due to a parity violating weak interactions) are different as well [4,5] and can be detected in spectroscopic experiments [5–7]. In this regard, the search for new phenomena and systems where the identity of enantiomers’ properties is violated is of great scientific importance.

The self-assembly of peptides into hierarchically and highly symmetric structures such as nanospheres, nanotubes, and nanoribbons has attracted considerable attention from researchers and has been intensively studied in supramolecular chemistry and nanotechnology for the last two decades [8–11]. Diphenylalanine (H-Phe-Phe-OH, FF) is one of the most studied aromatic dipeptides. The chirality of FF monomers determines the kinetics

of the peptide nanotubes' (PNT) self-assembly and their morphology [12]. The helical symmetry of FF PNTs causes significant intrinsic polarization [13] and endows them with a unique combination of mechanical [14,15], electronic [16,17], and optical [18–21] properties, as well as a strong piezoelectric effect useful for various applications [22–24].

The structure and properties of FF PNTs of different chiralities were studied by various authors experimentally and through computer modeling [12,13,25–27]. In our recent works [12,26,27], we have developed computer models of FF PNT structures based on the experimental crystallographic data obtained by X-ray diffraction [12,28] and used them for calculating the polar and piezoelectric properties of FF PNTs [12,26,27,29,30].

Although some interesting experimental works are devoted to the photoelectronic properties of FF PNTs [17–21,31], their computational study is still not sufficient and systematic [17,21]. For example, in Ref. [31] the photoferroelectric effects were considered, but the computer model used there was based on the  $\beta$ -sheet conformation of phenylalanine amino acid (F), while the latest experimental X-ray data [12,28] convincingly showed that FF PNTs self-assemble into  $\alpha$ -helices of L- and D-chirality.

In this work, we tried to fill this knowledge gap and carried out the computer modeling and quantum chemical calculations of photoelectronic properties of FF PNTs using  $\alpha$ -helix models from our previous works [12,26,27].

## 2. Computational Details, Models, and Methods

### 2.1. Basic Models of FF PNTs

The models of FF PNTs of L- and D-chiralities used in this work are based on experimental X-ray data and are available in the Cambridge Crystallographic Data Center [32]: CCDC 1853771 for D-FF [12] and CCDC 16340 for L-FF [28] (Figure 1a,c). Two consequent coils of the helices were simulated and then converted to the HyperChem workspace [33] using Jmol and OpenBabel software (Figure 1b,d), similar to how it was performed in our previous works [12,26,27,30].

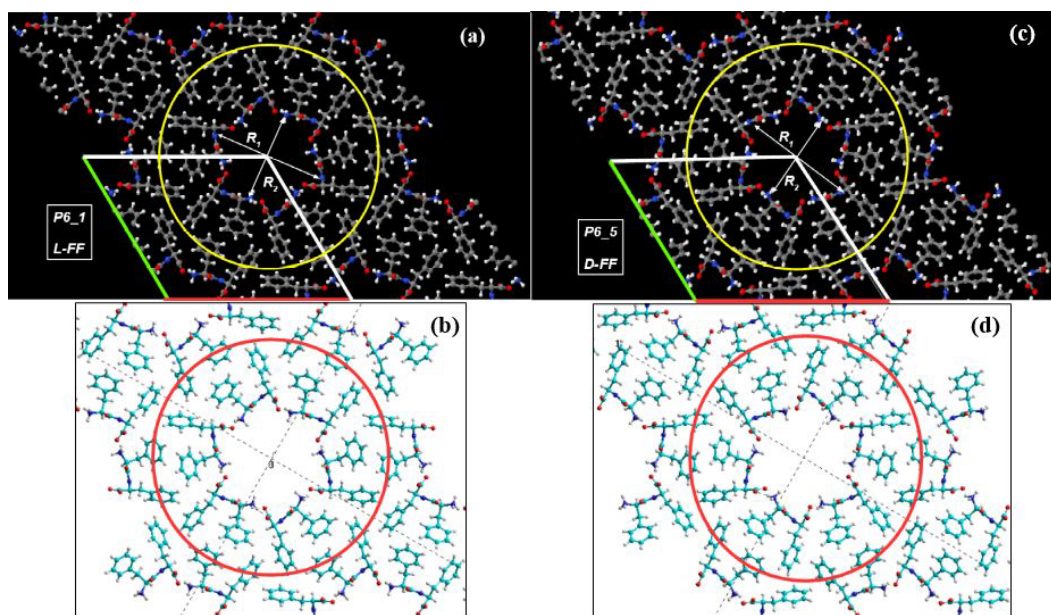


**Figure 1.** Original models of FF PNTs of different chiralities: (a) L-FF, (c) D-FF, and (b,d) the same models converted to the HyperChem workspace. Yellow and red circles denote the individual FF coil in the PNT structure. Reproduced with permission from [27]; Springer Nature, 2022.

These models were used earlier to study the self-assembly process of FF PNTs [12] and their polar properties [13]. The dipole moments  $D_i$  of individual dipeptides in PNTs form left- or right-handed helices and thus originate a nonzero total polarization of the nanotubes (Figure 2).

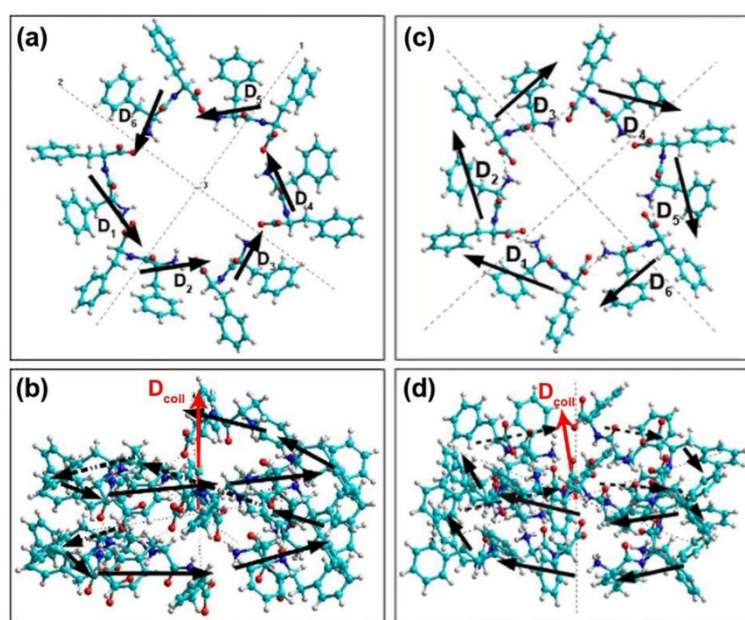


**Figure 2.** Two-coil fragments of the self-assembled FF PNTs in the HyperChem workspace with the denoted dipole moments of individual dipeptides,  $D_i$ , and the total dipole moments,  $D_{coil}$ , for (a,b) D-FF and (c,d) L-FF [13]. Dotted lines show inertial axes of the structures roughly coincided with their crystallographic axes.

It is important to note that the models were used without additional geometry optimization. We deliberately omitted this step since we used experimentally determined crystal data for both L-FF and D-FF nanotubes [12,28]. Additional optimization by the computational algorithms leads to aligning the ends of a helix step, thus breaking the inherent chirality of the nanotubes. This was shown in our previous work [34], where the optimization was performed. Moreover, the total energy of optimized rings appeared to be somewhat larger than that of the experimental ones, although the difference in total energies of D-FF and L-FF rings remains even after the optimization [34]. Therefore, the results presented here do not depend on the calculation method and thus are unlikely related to the calculation error.

## 2.2. Calculation Methods

The electronic energy levels of the FF PNT models with and without external electric field were calculated using quantum-chemical semiempirical methods AM1 and PM3 implemented in HyperChem 8.0 [33] and PM7 and PM6-D3H4 methods in MOPAC 2016 software [35] in the restricted Hartree-Fock (RHF) approximation.

## 3. Results and Discussion

### 3.1. Electronic Energy Levels without an Electric Field

Figure 3 shows the models of L-FF and D-FF PNTs with the calculated positions of the electronic molecular orbitals for the ground state (highest occupied molecular orbital—HOMO) and the first excited state (lowest unoccupied molecular orbital—LUMO). These molecular models consisting of two coils of helical FF PNTs were constructed earlier [26] based on the crystallographic unit cells obtained from X-ray data [12,28]. The distances between coils are equal to the unit cell parameter along the  $c$ -axis:  $c = 5.456 \text{ \AA}$  for L-FF PNT [28] and  $c = 5.441 \text{ \AA}$  for D-FF PNT [12]. The electron photoexcitation leads to the electronic wave cloud shift from the HOMO to the LUMO state at the distance equal to the corresponding  $c$  parameters along the PNT axis.

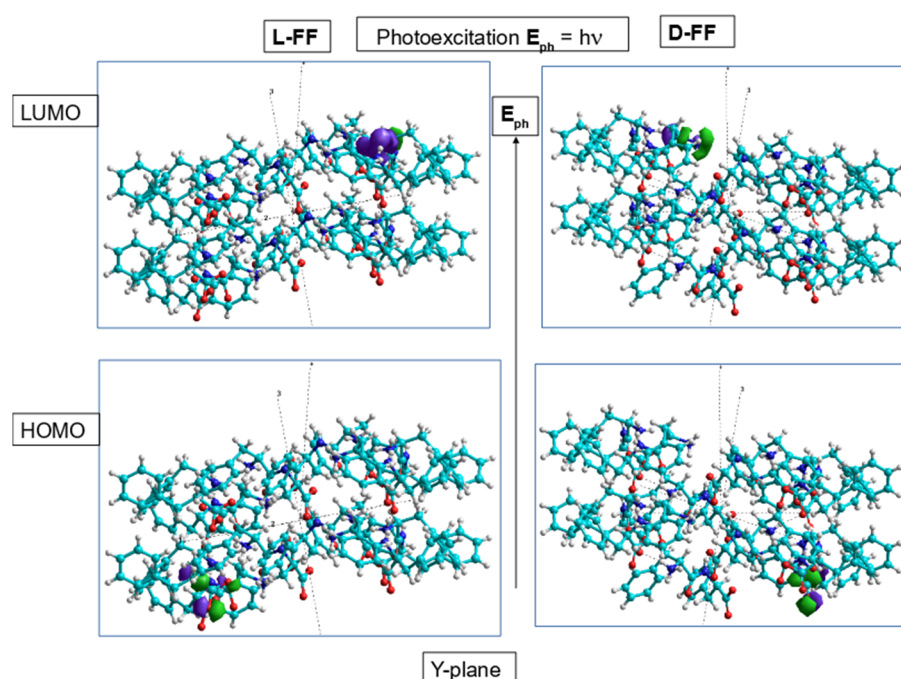


**Figure 3.** Two-coil models of FF PNT with different initial chirality L-FF and D-FF with electron molecular orbitals HOMO and LUMO computed by AM1/PM3 methods in RHF approximation.

The values of the HOMO and LUMO energy levels without an external electric field and calculated using different methods are presented in Table 1. Separately, for L-FF, as well as for D-FF PNTs, AM1 and PM3 methods implemented in the HyperChem package provide similar values of energy levels. At the same time, all methods, including more modern and precise methods PM6-D3H4 and PM7, demonstrate noticeably higher HOMO and LUMO energies for D-FF models than those of L-FF. This difference can be related to variations in the hydrogen bonds network in L-FF and D-FF PNTs, which also influences their self-assembly kinetics [12].

**Table 1.** Comparison of electron energy levels and the zero-field  $E_{g0}$  for FF PNTs calculated in this work by different methods without electric field and data obtained in other works.

Type/Method	$E_{HOMO}$ , eV	$E_{LUMO}$ , eV	$E_{g0}$ , eV	$\lambda$ , nm
D-FF/PM7	−6.085	−2.104	3.981	312
L-FF/PM7	−6.167	−2.201	3.966	313
D-FF/PM6-D3H4	−6.351	−2.731	3.620	343
L-FF/PM6-D3H4	−6.407	−2.835	3.572	348
D-FF/PM3/AM1	−5.924	−2.349	3.575	347
L-FF/PM3/AM1	−5.941	−2.4996	3.441	360
L-FF/DFT [17]	—	—	4.48	c.a. 277
D-FF/Opt. abs. [21]	—	—	4.69	c.a. 264
L-FF/Opt. abs. [18]	—	—	3.35–4.13	300–370
L-FF/Photolum. [19]	—	—	4.0–4.13	300–310
L-FF/Photolum. [20]	—	—	4.0	c.a. 310

The zero-field band gap,  $E_{g0}$ , was calculated as a difference between  $E_{LUMO}$  and  $E_{HOMO}$  energies:

$$E_{g0} = E_{LUMO} - E_{HOMO}. \quad (1)$$

The obtained values are presented in Table 1. For all calculation methods used, the band gap for D-FF PNTs is higher than that for L-FF. The  $E_{g0}$  values calculated by the PM7 method are closer to the data observed in experiment 4.0–4.69 eV (Table 1).

The band gap can be converted to the absorption edge,  $\lambda$ , and vice versa using the equation:

$$E_{g0} = hc/\lambda, \quad (2)$$

where  $h$  is the Planck constant, and  $c$  is the vacuum speed of light. For FF PNTs of both chiralities, all methods provide  $\lambda$  in the ultraviolet A range (UV-A, 315–400 nm), which are close to the values of 300–370 nm obtained in optical absorption experiments [18].

The obtained difference in  $E_{g0}$  values between L-FF and D-FF models is about 0.134 eV for the AM1 method and about 0.015 eV for PM7 (Table 1). A similar trend is observed in optical absorption experiments [18,21], which show that the band gap for D-FF PNTs is about 0.56 eV bigger than those of L-FF (Table 1). This difference may be related to a weak difference in electronic and vibrational levels similar to what was observed for 1-indanol chiral molecules [7]. However, to verify this hypothesis, additional precise experiments on optical absorption and photoluminescence performed under the same conditions should be conducted.

Another possible mechanism of the observed difference in the band gaps of L- and D-FF PNTs is the effect of an intrinsic electric field that existed in polar crystals such as piezo- or ferroelectrics [36–38]. Different dipole moments observed for L- and D-FF PNTs [31] indicate nonequivalent charge distribution in these PNTs, thus creating different intrinsic electric fields. The effect of this field is considered in detail below.

### 3.2. Influence of the External Electric Field

First, the effect of an external electric field on the photoelectronic properties was studied using the PM7 and AM1 methods. An axial electric field,  $E_z$ , in the range from −0.15 to +0.15 V/Å was applied to the FF PNTs models, and the variations of the HOMO and LUMO energy levels were determined. Then, the values of the band gap were calculated using Equation (1).

HOMO and LUMO energy levels demonstrate linear dependence on the applied electric field but with opposite slopes (Figure 4). For the positive direction of the applied  $E_z$  (codirected with the PNT's Z-axis),  $E_{LUMO}$  values increases, whereas  $E_{HOMO}$  decreases, and vice versa for the negative  $E_z$  direction. PM7 and AM1 methods provide slightly different values of  $E_{LUMO}$  and  $E_{HOMO}$ , although PM7 is more recent and may be closer to experiments. The difference between  $E_{LUMO}$  and  $E_{HOMO}$  values for L- and D-FF PNTs is close to that observed for a zero-field case (Table 1) for all studied  $E_z$ . The slopes for  $E_{LUMO}$  and  $E_{HOMO}$  are about −4.33 and 3.52 eV/(V/Å) for the PM7 method and −3.92 and 3.49 eV/(V/Å) for AM1.

Under the applied electric field, the band gap demonstrates a linear behavior similar to  $E_{LUMO}$  (Figure 4). Again, the values of  $E_g$  are different for the PM7 and AM1 methods, but they are close for L- and D-FF PNTs. The slope values,  $\alpha$ , are the following:

- (1) for the AM1 method:  $\alpha_1 = 7.182 \text{ eV}/(\text{V}/\text{\AA})$  for L-FF and  $\alpha_3 = 7.412 \text{ eV}/(\text{V}/\text{\AA})$  for D-FF;
- (2) for the PM7 method:  $\alpha_2 = 7.774 \text{ eV}/(\text{V}/\text{\AA})$  for L-FF and  $\alpha_4 = 7.853 \text{ eV}/(\text{V}/\text{\AA})$  for D-FF.

These results demonstrate the possibility of tuning the band gap of FF PNTs in a wide range simply by applying an external electric field along the nanotubes. This effect is similar to what is observed in layers of dichalcogenides of the MoS<sub>2</sub> type [39].

While the zero-field absorption edge  $\lambda \approx 310$ –350 nm (Table 1) lies at the edge of the UV-A and UV-B ranges, the application of  $E_z = -0.15 \text{ V}/\text{\AA}$  reduces  $E_g$  to c.a. 2.8 eV, which corresponds to the absorption edge  $\lambda \approx 443 \text{ nm}$  in the visible range. At the same time, the application of  $E_z = +0.15 \text{ V}/\text{\AA}$  shifts  $\lambda$  to the deep UV-C region ( $E_g \approx 5.1 \text{ eV}$ ,  $\lambda \approx 243 \text{ nm}$ ).

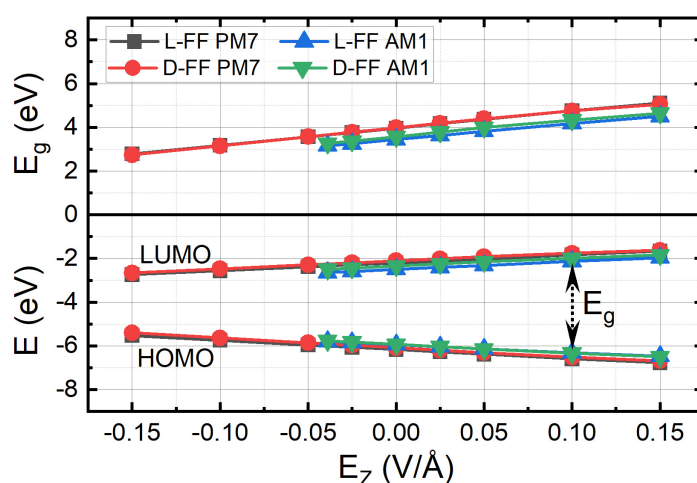


**Figure 4.** External electric field dependence of the electron energy levels HOMO and LUMO and the band gap  $E_g$  for L-FF and D-FF PNT structures calculated by different methods.

The blue photoluminescence observed earlier in FF PNTs was attributed to the quantum confinement phenomenon [18]. Our results show that the same effect can be achieved by the application of the electric field; moreover, it allows controlling the emission/absorption range of the FF PNTs. This effect is highly demanded for photoelectronic devices operating in the middle and near UV range (200–400 nm). Due to a strong absorption by the ozone layer in the atmosphere, sunlight with wavelengths of 200–300 nm cannot reach the earth's surface, thus creating a so-called black background. The solar-blind ultraviolet photodetectors (SBUV) operating in this spectral range are based mainly on wide-band-gap semiconductors such as gallium nitride or gallium oxide [40]. A similar photodetector can be made based on FF PNT structures. It can be used for monitoring ozone holes, fires, high-voltage transmission lines, etc.

Moreover, understanding the effect of external electric fields on the electronic and optical properties of FF PNTs is crucial for developing new optical and electronic devices, such as planar electro-optical modulators or composite nanostructures for energy generation. The nonlinear optical properties, second harmonic generation, and waveguiding ability of PNTs have been demonstrated recently [41,42].

### 3.3. Influence of the Intrinsic Electric Field

It is known that FF PNTs possess a strong dipole momentum  $D$  and the polarization  $P = 3.33556255 \times D_t/V_0$  (here,  $V_0$  is the van der Waals volume of the PNT's unit cell:  $V_0(\text{L-FF}) = 3365.6 \text{ Å}^3$ ,  $V_0(\text{D-FF}) = 3346.49 \text{ Å}^3$ ), aligned with the nanotube's axis Z (Table 2) [13]. This polarization, which is similar to the spontaneous polarization in ferroelectrics, produces a significant internal electric field  $E_p = P/\epsilon\epsilon_0$  [31,36–38], where  $\epsilon$  is the dielectric permittivity of FF PNTs, which is usually about 4 for the known protein structures, and  $\epsilon_0 = 8.85 \times 10^{-12} \text{ C}/(\text{V}\cdot\text{m})$  is the vacuum permittivity. A similar internal field that exists in ferroelectrics (the so-called depolarization field) causes a number of specific photoferroelectric and photovoltaic effects, and it is especially pronounced at the nanoscale [30,31,36–38].

**Table 2.** The polar properties of FF PNTs and the refined zero-field band gap values.

Type/ Method	$D$ , Debye	$P$ , $\text{C}/\text{m}^2$	$E_p$ , $\text{GV}/\text{m}$	$\alpha$ , $\text{eV}/(\text{GV}/\text{m})$	$E_{g0}$ , $\text{eV}$	$E_{g1}$ , $\text{eV}$	$E_{g2}$ , $\text{eV}$	$\Delta E_{ex}$ , $\text{eV}$	$\Delta\lambda_{ex}$ , $\text{nm}$
D-FF/PM7	146.60	0.146	4.126	0.785	3.981	5.600	4.923	0.677	30.5
L-FF/PM7	146.24	0.145	4.092	0.777	3.966	5.558	4.899	0.659	30.0
D-FF PM3/AM1	137.70	0.137	3.875	0.741	3.575	5.009	4.464	0.545	30.2
L-FF PM3/AM1	140.72	0.139	3.938	0.718	3.441	4.851	4.303	0.548	32.6

In particular, this additional intrinsic electric field codirected with the PNT's Z-axis affects the energy levels during the electrons' photoexcitation and, as a result, increases the band gap by the value:

$$\Delta E_{g1} = \frac{1}{2} \alpha E_P, \quad (3)$$

where  $\alpha$  is the  $E_g$  slope; these values were found in the previous section. The refined values of the band gap,  $E_{g1} = E_{g0} + \Delta E_{g1}$ , are presented in Table 2. These values are closer to those observed in experiments (Table 1) than  $E_{g0}$  obtained before. Thus, the internal electric field originated due to the nonzero polarization of FF PNTs plays a significant role in their photoelectronic properties, as in usual ferroelectrics [36–38].

Here, an external electric field  $E_z$  was considered to be zero. In the opposite case, the internal electric field  $E_P$  sums with or subtracts from the  $E_z$ , and the resulting energy levels and the band gap shift accordingly. Therefore, the resulting band gap value can be found as follows:

$$E_g = E_{g0} + \alpha(\frac{1}{2} E_P \pm E_z). \quad (4)$$

### 3.4. Exciton Formation and Photoluminescence

As soon as an electron occupies the excited LUMO state and a hole appears in the HOMO state, they form an exciton and create an additional electric field  $E_Q$  due to the charges separation. The value of this field can be estimated as  $E_Q = e/(4\pi\epsilon\epsilon_0\Delta z^2) \approx 1.2 \text{ GV/m}$ , where  $e$  is the elementary charge and the distance  $\Delta z \approx c = 5.45 \text{ \AA}$  (Figure 5a). This field is oriented opposite to the  $E_P$  and thus partially reduces the total internal electric field in the PNTs. Therefore, the exciton reduces the energy levels and the band gap by the value:

$$\Delta E_{ex} = \alpha(\frac{1}{2} E_P - E_Q). \quad (5)$$

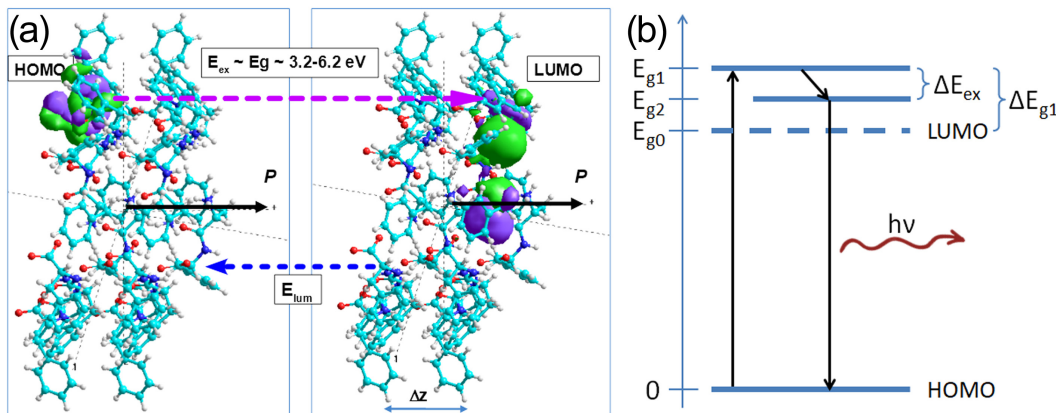


**Figure 5.** (a) Space configuration of the electronic clouds HOMO and LUMO and separation distance  $\Delta z$  between them for a D-FF PNT model. The polarization  $P$ , excitation energy  $E_{ex}$ , and luminescence energy  $E_{lum}$  are shown. Violet and blue dashed arrows show excitation and luminescence electron transitions. (b) The scheme of the energy levels in FF PNTs and luminescence transitions.

The values of  $\Delta E_{ex}$  and the refined band gap,  $E_{g2} = E_{g1} - \Delta E_{ex}$ , taking into account both the internal field and the exciton effect, are presented in Table 2. An average exciton correction leading to the “red” shift of the band gap is about 0.61 eV. This value is close to the exciton binding energy c.a. 0.34 eV determined in Ref. [21].

The photoluminescence occurs in FF PNTs when an electron transits between the LUMO excited level and the HOMO ground state (Figure 5b). The effects of the internal electric field and exciton formation change the position of the LUMO level and thus modify the wavelength of the emitted photons. While the internal electric field inherently exists in the PNTs, the exciton formation is an optional process, and, once it takes place, the photoluminescence wavelength is reduced by the value:

$$\Delta\lambda_{ex} = ch(E_g2^{-1} - E_g1^{-1}). \quad (6)$$

For all calculation methods, the values of  $\Delta\lambda_{ex}$  are about 30 nm for both L-FF and D-FF PNTs (Table 2). This value is consistent with previous experimental data [17–21].

#### 4. Conclusions

Thus, in the example of FF PNTs of different chiralities, we have demonstrated that symmetry and asymmetry [43,44] play an important role at various levels of structural organization from individual molecules to supramolecular structures [45–47] and reveal themselves in photoelectronic properties. Computer modeling and quantum chemical calculations allowed us to calculate the LUMO and HOMO energy levels and the band gap in hierarchically self-assembling FF PNTs of different chiralities with and without applied electric fields. Although the difference between  $E_g$  of L-FF and D-FF PNTs is small, it exists and can be attributed to the effect of the internal electric field caused by the ferroelectric-like polarization in PNTs. This internal electric field can be responsible for various photoferroelectric phenomena similar to what is observed in other ferroelectric nanomaterials.

Application of the axial external electric field significantly modifies the band gap and, thus, the absorption edge of the PNTs. The field of  $\pm 0.15$  V/Å shifts the absorption edge from the deep UV-C region to the visible one. The field could be created by the ferroelectric polymer layers such as PVDF and P(VDF-TrFE). The band gap range of 3.1–4.9 eV corresponds to the solar-blind ultraviolet range (400–253 nm) absorbed by the ozone layer. Therefore, the FF PNTs and their composites could be used as elements of new cost-effective, self-powered, and flexible solar-blind ultraviolet photodetectors and other electro-optic and electronic devices.

The exciton formation reduces the band gap and thus can be used for fine-tuning the photoluminescence and photovoltaic properties of FF PNTs. Further in-depth computational studies of various properties of FF PNTs based on the combination of DFT and semiempirical calculations may open new ways for the practical use of FF PNTs.

**Author Contributions:** Conceptualization, V.B. and V.F.; investigation, H.S. and T.L.; formal analysis, P.Z. and S.K.; writing—original draft preparation, V.B. and P.Z.; supervision, E.P. and V.F. All authors have read and agreed to the published version of the manuscript.

**Funding:** This research received no external funding.

**Data Availability Statement:** The data presented in this study are available on request from the corresponding author.

**Acknowledgments:** The authors are grateful to the Russian Foundation for Basic Research, RFBR (grants 19-01-00519\_A and 20-51-53014\_GFEN\_A). This work was developed within the scope of the project CICECO-Aveiro Institute of Materials, UIDB/50011/2020, UIDP/50011/2020, and LA/P/0006/2020, supported through the FCT/MEC (PIDDAC). Part of this work was supported by national funds (OE), through FCT—Fundação para a Ciência e a Tecnologia, I.P., in the scope of the framework contract foreseen in the numbers 4, 5, and 6 of article 23, of the Decree-Law 57/2016, of 29 August, changed by Law 57/2017, of 19 July. The computational parts of the study were completed within the framework of the noncommercial agreement on scientific and technical cooperation between the Institute of Mathematical Problems of Biology (IMPB)—branch of KIAM RAS, Russia and the Department of Physics of the University of Aveiro, Portugal. The authors are grateful for the opportunity to perform calculations using the computer cluster of IMPB RAS and the K-60 hybrid supercomputer installed at the KIAM RAS Shared Use Center.

**Conflicts of Interest:** The authors declare no conflict of interest.

#### References

1. Sallembien, Q.; Bouteiller, L.; Crassous, J.; Raynal, M. Possible chemical and physical scenarios towards biological homochirality. *Chem. Soc. Rev.* **2022**, *51*, 3436–3476. [[CrossRef](#)] [[PubMed](#)]
2. Jacques, J.; Collet, A.; Wilen, S.H. *Enantiomers, Racemates and Resolutions*; Krieger Publishing Company: Malabar, FL, USA, 1994.
3. Naaman, R.; Waldeck, D.H. Spintronics and Chirality: Spin Selectivity in Electron Transport Through Chiral Molecules. *Annu. Rev. Phys. Chem.* **2015**, *66*, 263–281. [[CrossRef](#)]

4. Letokhov, V.S. On difference of energy levels of left and right molecules due to weak interactions. *Phys. Lett. A* **1975**, *53*, 275–276. [[CrossRef](#)]
5. Quack, M.; Stohner, J.; Willeke, M. High-Resolution Spectroscopic Studies and Theory of Parity Violation in Chiral Molecules. *Ann. Rev. Phys. Chem.* **2008**, *59*, 741–769. [[CrossRef](#)] [[PubMed](#)]
6. Vitanov, N.V.; Drewsen, M. Highly Efficient Detection and Separation of Chiral Molecules through Shortcuts to Adiabaticity. *Phys. Rev. Lett.* **2019**, *122*, 173202. [[CrossRef](#)] [[PubMed](#)]
7. Lee, J.H.; Bischoff, J.; Hernandez-Castillo, A.O.; Sartakov, B.; Meijer, G.; Eibenberger-Arias, S. Quantitative Study of Enantiomer-Specific State Transfer. *Phys. Rev. Lett.* **2022**, *128*, 173001. [[CrossRef](#)]
8. Makam, P.; Gazit, E. Minimalistic peptide supramolecular co-assembly: Expanding the conformational space for nanotechnology. *Chem. Soc. Rev.* **2018**, *47*, 3406. [[CrossRef](#)]
9. Yuan, C.; Ji, W.; Xing, R.; Li, J.; Gazit, E.; Yan, X. Hierarchically oriented organization in supramolecular peptide crystals. *Nat. Rev. Chem.* **2019**, *3*, 567–588. [[CrossRef](#)]
10. Zelenovskii, P.S.; Romanyuk, K.; Liberato, M.S.; Brandão, P.; Ferreira, F.F.; Kopyl, S.; Mafra, L.M.; Alves, W.A.; Kholkin, A.L. 2D Layered Dipeptide Crystals for Piezoelectric Applications. *Adv. Funct. Mater.* **2021**, *31*, 2102524. [[CrossRef](#)]
11. Raymond, D.M.; Nilsson, B.L. Multicomponent peptide assemblies. *Chem. Soc. Rev.* **2018**, *47*, 3659. [[CrossRef](#)]
12. Zelenovskiy, P.S.; Nuraeva, A.S.; Kopyl, S.; Arkhipov, S.G.; Vasilev, S.G.; Bystrov, V.S.; Gruzdev, D.A.; Waliczek, M.; Svitlyk, V.; Shur, V.Y.; et al. Chirality-dependent growth of self-assembled diphenylalanine microtubes. *Cryst. Growth Des.* **2019**, *19*, 6414–6421. [[CrossRef](#)]
13. Bystrov, V.; Sidorova, A.; Lutsenko, A.; Shpigun, D.; Malyshko, E.; Nuraeva, A.; Zelenovskiy, P.; Kopyl, S.; Kholkin, A. Modeling of Self-Assembled Peptide Nanotubes and Determination of Their Chirality Sign Based on Dipole Moment Calculations. *Nanomaterials* **2021**, *11*, 2415. [[CrossRef](#)] [[PubMed](#)]
14. Kol, N.; Adler-Abramovich, L.; Barlam, D.; Shneck, R.Z.; Gazit, E.; Roucco, I. Self-Assembled Peptide Nanotubes Are Uniquely Rigid Bioinspired Supramolecular Structures. *Nano Lett.* **2005**, *5*, 1343–1346. [[CrossRef](#)] [[PubMed](#)]
15. Zelenovskiy, P.; Kornev, I.; Vasilev, S.; Kholkin, A. On the origin of the great rigidity of self-assembled diphenylalanine nanotubes. *Phys. Chem. Chem. Phys.* **2016**, *18*, 29681. [[CrossRef](#)] [[PubMed](#)]
16. Tao, K.; Makam, P.; Aizen, R.; Gazit, E. Self-assembling peptide semiconductors. *Science* **2017**, *358*, eaam9756. [[CrossRef](#)]
17. Akdim, B.; Pachter, R.; Naik, R.R. Self-assembled peptide nanotubes as electronic materials: An evaluation from first-principles calculations. *Appl. Phys. Lett.* **2005**, *106*, 183707. [[CrossRef](#)]
18. Amdursky, N.; Molotskii, M.; Aronov, D.; Adler-Abramovich, L.; Gazit, E.; Rosenman, G. Blue luminescence based on quantum confinement at peptide nanotubes. *Nano Lett.* **2009**, *9*, 3111–3115. [[CrossRef](#)]
19. Gan, X.; Wu, X.; Zhu, X.; Shen, J. Light-induced ferroelectricity in bioinspired self-assembled diphenylalanine nanotubes/microtubes. *Angew. Chem. Int. Ed.* **2013**, *52*, 2055–2059. [[CrossRef](#)]
20. Gan, Z.; Wu, X.; Zhang, J.; Zhu, X.; Chu, P.K. In Situ Thermal Imaging and Absolute Temperature Monitoring by Luminescent Diphenylalanine Nanotubes. *Biomacromolecules* **2013**, *14*, 2112–2116. [[CrossRef](#)]
21. Nikitin, T.; Kopyl, S.; Shur, V.Y.; Kopelevich, V.Y.; Kholkin, A.L. Low-temperature photoluminescence in self-assembled diphenylalanine microtubes. *Phys. Lett. A* **2016**, *380*, 1658–1662. [[CrossRef](#)]
22. Nguyen, V.; Zhu, R.; Jenkins, K.; Yang, R. Self-assembly of diphenylalanine peptide with controlled polarization for power generation. *Nat. Commun.* **2016**, *7*, 13566. [[CrossRef](#)] [[PubMed](#)]
23. Jenkins, K.; Kelly, S.; Nguyen, V.; Wu, Y.; Yang, R. Piezoelectric diphenylalanine peptide for greatly improved flexible nanogenerators. *Nano Energy* **2022**, *51*, 317–323. [[CrossRef](#)]
24. Vasilev, S.; Zelenovskiy, P.; Vasileva, D.; Nuraeva, A.; Shur, V.Y.; Kholkin, A.L. Piezoelectric properties of diphenylalanine microtubes prepared from the solution. *J. Phys. Chem. Solids* **2016**, *93*, 68. [[CrossRef](#)]
25. Carny, O.; Gazit, E. Creating Prebiotic Sanctuary: Self-Assembling Supramolecular Peptide Structures Bind and Stabilize RNA. *Orig. Life Evol. Biosph.* **2011**, *41*, 121–132. [[CrossRef](#)]
26. Bystrov, V.; Coutinho, J.; Zelenovskiy, P.; Nuraeva, A.; Kopyl, S.; Zhulyabina, O.; Tverdislov, V. Structures and properties of the self-assembling diphenylalanine peptide nanotubes containing water molecules: Modeling and data analysis. *Nanomaterials* **2020**, *10*, 1999. [[CrossRef](#)] [[PubMed](#)]
27. Bystrov, V.S.; Filippov, S.V. Molecular modelling and computational studies of peptide diphenylalanine nanotubes, containing waters: Structural and interactions analysis. *J. Mol. Model.* **2022**, *28*, 81. [[CrossRef](#)]
28. Görbitz, C.H. Nanotube formation by hydrophobic dipeptides. *Chem. Eur. J.* **2001**, *7*, 5153. [[CrossRef](#)]
29. Bystrov, V.S.; Paramonova, E.V.; Bdikin, I.; Kopyl, S.; Heredia, A.; Pullar, R.; Kholkin, A. BioFerroelectricity: Diphenylalanine Peptide Nanotubes Computational Modeling and Ferroelectric Properties at the Nanoscale. *Ferroelectrics* **2012**, *440*, 3–24. [[CrossRef](#)]
30. Bystrov, V.S.; Coutinho, J.; Zhulyabina, O.A.; Kopyl, S.A.; Zelenovskiy, P.S.; Nuraeva, A.S.; Tverdislov, V.A.; Filippov, S.V.; Kholkin, A.L.; Shur, V.Y. Modeling and physical properties of diphenylalanine peptide nanotubes containing water molecules. *Ferroelectrics* **2021**, *574*, 78–91. [[CrossRef](#)]
31. Bystrov, V.S. Photoferroelectricity in di-phenylalanine peptide nanotube. *Comput. Condens. Matter* **2018**, *14*, 94–100. [[CrossRef](#)]
32. The Cambridge Crystallographic Data Centre (CCDC). Available online: <https://www.ccdc.cam.ac.uk/> (accessed on 17 December 2022).
33. HyperChem. Tools for Molecular Modeling; Release 8.0/01; Hypercube, Inc.: Gainesville, FL, USA, 2011.

34. Bystrov, V.S.; Kopyl, S.A.; Zelenovskiy, P.; Zhulyabina, O.A.; Tverdislov, V.A.; Salehli, F.; Ghermani, N.E.; Shur, V.Y.; Kholkin, A.L. Investigation of physical properties of diphenylalanine peptide nanotubes having different chiralities and embedded water molecules. *Ferroelectrics* **2018**, *525*, 168–177. [CrossRef]
35. Stewart, J.J.P. Stewart Computational Chemistry. MOPAC2016 [Electronic Resource], Colorado Springs, CO, USA. 2016. Available online: <http://openmopac.net/MOPAC2016.html> (accessed on 30 October 2022).
36. Fridkin, V.M. *Photoferroelectrics*; Springer: New York, NY, USA, 1979.
37. Fridkin, V.M.; Ducharme, S. *Ferroelectricity at the Nanoscale; Basic and Applications*; Springer: New York, NY, USA; London, UK, 2014.
38. Bystrov, V.S.; Fridkin, V.M. Two-dimensional ferroelectrics and homogeneous switching. *Phys. Usp.* **2020**, *63*, 417–439.
39. Wang, X.; Wang, P.; Wang, J.; Hu, W.; Zhou, X.; Guo, N.; Huang, H.; Sun, S.; Shen, H.; Lin, T.; et al. Ultrasensitive and Broadband MoS<sub>2</sub> Photodetector Driven by Ferroelectrics. *Adv. Mater.* **2015**, *27*, 6575–6581. [CrossRef] [PubMed]
40. Zhang, X.; Wang, L.; Wang, X.; Chen, Y.; Shao, Q.; Wu, G.; Wang, X.; Lin, T.; Shen, H.; Wang, J.; et al. High-performance β-Ga<sub>2</sub>O<sub>3</sub> thickness dependent solar blind photodetector. *Opt. Express* **2020**, *28*, 4169–4177. [CrossRef] [PubMed]
41. Handelman, A.; Apter, B.; Turko, N.; Rosenman, G. Linear and nonlinear optical waveguiding in bio-inspired peptide nanotubes. *Acta Biomater.* **2016**, *30*, 72–77. [CrossRef] [PubMed]
42. Handelman, A.; Lavrov, S.; Kudryavtsev, A.; Khatchatourians, A.; Rosenberg, Y.; Mishina, E.; Rosenman, G. Nonlinear Optical Bioinspired Peptide Nanostructures. *Adv. Optical Mater.* **2013**, *1*, 875–884. [CrossRef]
43. Weyl, H. *Symmetry*; Princeton University Press: Princeton, NJ, USA, 1952.
44. Kane, G. *Supersymmetry and Beyond: From the Higgs Boson to the New Physics*; Basic Books: New York, NY, USA, 2013.
45. Holmstedt, B.; Frank, H.; Testa, B. (Eds.) *Chirality and Biological Activity*; Liss: New York, NY, USA, 1990.
46. Yashima, E.; Ousaka, N.; Taura, D.; Shimomura, K.; Ikai, T.; Maeda, K. Supramolecular Helical Systems: Helical Assemblies of Small Molecules, Foldamers, and Polymers with Chiral Amplification and Their Functions. *Chem. Rev.* **2016**, *116*, 13752–13990. [CrossRef] [PubMed]
47. Tverdislov, V.A. Chirality as a primary switch of hierarchical levels in molecular biological systems. *Biophysics* **2013**, *58*, 128–132. [CrossRef]

**Disclaimer/Publisher’s Note:** The statements, opinions and data contained in all publications are solely those of the individual author(s) and contributor(s) and not of MDPI and/or the editor(s). MDPI and/or the editor(s) disclaim responsibility for any injury to people or property resulting from any ideas, methods, instructions or products referred to in the content.